Hindawi
Advances in Condensed Matter Physics
Volume 2019, Article ID 5960587, 8 pages
https://doi.org/10.1155/2019/5960587

Research Article

Effect of Deposition Time on the Optoelectronics Properties of PbS Thin Films Obtained by Microwave-Assisted Chemical Bath Deposition

Enue Barrios-Salgado,[1] **Y. Rodríguez-Lazcano**,[1] **Juan Pablo Pérez-Orozco**,[2] **J. Colin**,[3] **P. Altuzar**,[4] **J. Campos**,[4] **and David Quesada**[5]

[1] *Unidad Académica de Ciencias Básicas e Ingenierías, Universidad Autónoma de Nayarit, Ciudad de la Cultura "Amado Nervo" S/N, 63155, Tepic, NAY, Mexico*
[2] *Departamento de Ingeniería Química y Bioquímica, Instituto Tecnológico de Zacatepec, Tecnológico Nacional de México, Calzada Tecnológico #27, Col. Centro, 62780, Zacatepec, MOR, Mexico*
[3] *Facultad de Ciencias Químicas e Ingeniería, Universidad Autónoma del Estado de Morelos, Av. Universidad 1001, Col. Chamilpa, 62209, Cuernavaca, MOR, Mexico*
[4] *Instituto de Energías Renovables, Universidad Nacional Autónoma de México, 62580, Temixco, MOR, Mexico*
[5] *Department of Mathematics, Miami Dade College, Wolfson Campus, Miami, FL 33132, USA*

Correspondence should be addressed to Y. Rodríguez-Lazcano; yamilet.lazcano@uan.edu.mx

Received 26 November 2018; Revised 5 February 2019; Accepted 13 February 2019; Published 3 March 2019

Guest Editor: Hong Fang

PbS thin films with thickness between 100 and 150 nm were grown for the first time by microwave-assisted chemical bath deposition in a commercial automated system with deposition times not exceeding 5 min. X-ray diffraction analysis shows that the thin films have cubic rock salt type structure with good crystallinity. The grain size increased from 18 to 20 nm, as the deposition time increased. Energy dispersive X-ray results confirm that the films are stoichiometric. Optical measurements show that thin films have relatively high absorption coefficients between 10^4 and 10^5 cm-1 in the visible range. In addition, the films exhibit a direct gap, within the energy range from 1.0 to 1.35 eV. The electrical properties, such as conductivity, the Seebeck coefficient, carrier concentration, and carrier mobility, are discussed.

1. Introduction

Lead sulfide (PbS) is an important IV–VI semiconductor material with technological applications including infrared detectors [1] and absorbers in thin film solar cells [2, 3]. Different methods have been used to synthesize PbS; they include chemical bath deposition (CBD) [4, 5], spray pyrolysis [6], pulsed laser deposition [7], vacuum evaporation [8], chemical vapor deposition (CVD) [9], ultrasound [10], and electrodeposition [11].

Studies of PbS thin films obtained by CBD showed that this compound has a band gap (Eg) within the range of energies from around 1.39-1.55 to 2.38-2.75 eV, an electrical resistivity of $10^5\Omega$ cm, and a preference orientation along the (111) or (200) planes with grain sizes about 20 or 34 nm depending on the temperature and/or formulation used [5, 12, 13]. The authors in [14] prepared PbS films by CBD at room temperature for different deposition times (from 60 to 300 min) using lead acetate as a source of Pb ions, thiourea to produce S ions, and triethanolamine as the complexing agent in water. As a result, grown films showed that Eg decreases from 0.52 to 0.38 eV, as deposition time increases.

Besides the traditional set-up for CBD, PbS thin films have been also deposited by CBD under the influence of UV radiation [14] and microwave radiation [15–19]. Nanocrystalline PbS thin films have been reported using a microwave-assisted chemical bath deposition method with deposition times from 30 to 120 min showing a p-type conductivity

[15]. X-ray diffraction patterns show cubic rock salt (NaCl) structure with preference crystalline orientation along (111) or (200) depending on the deposition time. Moreover, as the deposition time increases, the particle size increases from 13 to 23 nm, while both the electrical resistivity and the band gap Eg decrease from 380 to 347 Ω cm and from 2.7 to 1.6 eV, respectively. The synthesis of PbS nanocrystals in an ethanol solvent for 20 min by microwave heating was reported in [16] with size around 10 nm approximately. Additionally, the pure cubic phase of PbS nanocrystals has been grown by applying a microwave radiation for 30 min using ethanol, distilled water, ethylene glycol, and polyethylene glycol-200 as solvents and lead acetate and thiourea as lead and sulfur sources, respectively [17]. These films show a direct transition with an optical band gap of 3.49 eV. The nanoparticles of PbS were prepared in a domestic microwave oven with different sulfur sources and $Pb(NO_3)_2$ as lead source [18].

The microwave-assisted chemical bath deposition (MA-CBD) is a simple, quite fast, and energy-efficient method to obtain thin films [20]. The heating is generated from inside the solution through microwave irradiation, which causes a homogenous distribution of temperature within the solution and accelerates the growth rate by accelerating the film's reaction kinetics [21, 22].

As far as we know, this is the first time that thin films of PbS are reported to be grown by MA-CBD with deposition times not exceeding 5 min in a commercial automated system. In this work, the PbS thin films were synthesized using thioacetamide as sulfur source at different deposition times. The structural, optical, and electrical properties of the thin films were analyzed.

2. Materials and Methods

2.1. Thin Film Deposition. PbS thin films were grown by microwave-assisted chemical bath deposition, following the chemical formulation reported previously [23]. A solution containing 5 ml of $Pb(NO_3)_2$ 1 M, 20 ml of NaOH 1 M, 6 ml of CH_3CSNH_2 1 M, 4 ml of $(HOCH_2CH_2)_3N$ 1 M, and distilled water was prepared. Typical microscope glass slides were cut to obtain 75 x 8 x 2 mm substrates. One substrate was introduced each time into the vial containing the chemical solution. Then, the vial was placed in the Anton Paar Microwave Synthesis Reactor Monowave 300 (2.4 GHz). The deposition was carried out at 40°C for 2, 3, and 4 min. Finally, the samples were taken out of the solution and washed with distilled water. The thicknesses of the films were 100, 130, and 150 nm for 2, 3, and 4 min, respectively.

2.2. Characterization. Films' thickness was measured on an XP-200 Ambios Technology profilometer. X-ray diffraction (XRD) patterns were recorded with Cu-K_α radiation on a Rigaku Ultima IV diffractometer with grazing incidence of 1.0° with the sample plane. A field effect scanning electron microscope, Hitachi-FESEM S-5500, was used to analyze the surface morphology of the films. Chemical composition was analyzed in an Oxford x-act energy dispersive X-ray spectrum (EDX) analyzer attached to a Hitachi-SEM SU1510. Optical transmittance and specular reflectance spectra were measured in a JASCO V-670 spectrometer using air or an aluminized mirror as reference, respectively. For the electrical measurements we used a Keithley 230 programmable voltage source and a Keithley 619 electrometer. A pair of carbon electrodes (5 mm length and 5 mm separation) were painted on the film surface, at which the I-V characteristics have ohmic behavior. Photocurrent response curves were done with a bias (V) of 10 V applied across the electrodes. The current (I) in the sample is recorded at each 0.5 s for the first 20 s in the dark, the next 20 s under 1000 W/m^2 provided by a tungsten halogen lamp, and the last 20 s after switching off the illumination. Thermoelectric measurements were done by a microvoltmeter/scanning thermometer Keithley 740 and the DC power supply with two Peltier elements to establish a difference of temperature. The activation energy for the electrical conductivity was evaluated in the temperature range between 298 and 363 K.

3. Results and Discussion

3.1. Reaction Mechanism. The reaction mechanism for forming PbS thin films is as follows:

Pb^{2+} ions result from $Pb(NO_3)_2$, through the reactions shown below [24]:

$$\begin{aligned} Pb(NO_3)_2 + 2NaOH &\longrightarrow Pb(OH)_2 + 2NaNO_3 \\ Pb(OH)_2 + 2NaOH &\longrightarrow Na_2[Pb(OH)_4] \\ [Pb(OH)_4]^{2-} &\longrightarrow Pb^{2+} + 4OH^- \end{aligned} \quad (1)$$

Additionally, the hydrolysis of thioacetamide, CH_3CSNH_2, takes place in the solution which releases S^{2-} ions as follows [25]:

$$\begin{aligned} CH_3CSNH_2 + H_2O &\longrightarrow CH_3CONH_2 + H_2S \\ H_2S + H_2O &\longrightarrow H_3O^+ + HS^- \\ HS^- + H_2O &\longrightarrow H_3O^+ + S^{2-} \end{aligned} \quad (2)$$

When the ionic product of Pb^{2+} and S^{2-} ions exceeds the solubility product of PbS ($1.1x10^{-29}$), the insoluble solid PbS precipitate is produced:

$$Pb^{2+} + S^{2-} \longrightarrow PbS \quad (3)$$

Microwave radiation used for the MA-CBD provides the necessary energy for the PbS formation. While describing the kinetics of the reaction, it is worth noticing that the heating is due to the interaction of the microwave radiation with the solution through two mechanisms [26, 27]. These mechanisms are related to the interaction of the microwave radiation with the ionic medium and with the polar solvent, that is, the water, which leads to a homogeneous distribution of the temperature inside the solution, not only accelerating the formation of the nuclei of PbS but also stimulating the growth of the crystals.

Table 1: Structural parameters as a function of deposition time.

Sample	2θ (deg)	FWHM (deg)	Grain size (nm)	Lattice constant (Å)	Interplanar spacing (Å)
2 min	30.01	0.4757	18.0	5.95	2.967
3 min	30.08	0.4303	19.9	5.94	2.970
4 min	30.05	0.4213	20.3	5.94	2.973

Table 2: Atomic percent of PbS thin films.

Sample	Atomic %	
	Pb	S
2 min	49.82	50.18
3 min	49.09	50.91
4 min	49.25	50.75

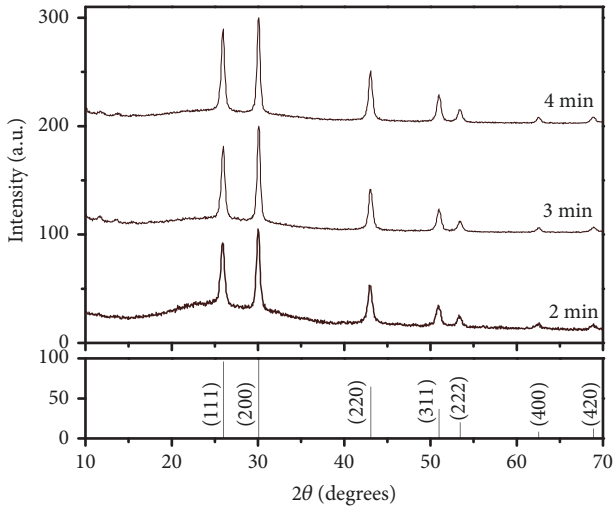

Figure 1: XRD patterns of PbS thin film as a function of deposition time.

3.2. Structural Properties. Figure 1 shows the X-ray diffraction patterns of the PbS thin films deposited by the MA-CBD technique at 40°C on glass substrates during 2, 3, and 4 min. XRD patterns clearly have diffraction peaks at 25.96°, 30.06°, 43.01°, 50.90°, 53.37°, 62.54°, and 68.90° which correspond to the (111), (200), (220), (311), (222), (400), and (420) Miller planes of cubic structure (Galena) PbS (PDF# 077-0244), respectively. These results indicate that the films are crystalline with cubic rock salt (NaCl) type structure.

The crystallite size (D) was calculated from the XRD spectrum using Scherrer's equation [28]:

$$D = \frac{0.94\lambda}{\beta \cos\theta}, \tag{4}$$

where θ is the Bragg diffraction angle, λ is the wavelength of X-ray radiation, and β is the full-width at half-maximum (FWHM) of the main peak (200) in the XRD pattern.

An increase in the grain size is observed as the deposition time increases. This leads to an improvement in the crystallinity of the samples. In addition, the FWHM of PbS thin films decreases with increasing deposition time, which supports the observed increase in crystallinity. These results are presented in Table 1.

The interplanar spacing (d) was taken from the (200) plane using the XRD equipment software. As can be seen in Table 1, the calculated interplanar spacing values are in good agreement with the 2.967 Å reported in the standard PDF# 077-0244.

The lattice constant, a, of the films for the cubic structure was calculated using the equation [29]

$$\frac{1}{d^2} = \frac{h^2 + k^2 + l^2}{a^2}, \tag{5}$$

where h, k, and l are the Miller indices and d is the interplanar spacing. The values of lattice constant are shown in Table 1. It is found that the lattice constant values obtained are in agreement with $a = 5.934$ Å as reported in PDF# 077-0244.

3.3. Surface Morphology and Chemical Composition. Figure 2 shows the SEM images of PbS thin films grown for 2, 3, and 4 min. The micrographs show granular structure with well-defined grain boundaries. Additionally, the films display homogenous surface morphology without microcracks and pinholes.

The characteristic peaks of S-K_α at 2.307 keV, Pb-M at 2.342 keV, and Pb-L_α at 10.550 keV are identified in the EDX spectra of the thin films along with those arising from the substrate (Na-K_α at 1.04 keV, Mg-K_α at 1.253 keV, Al-K_α at 1.486 keV, Si-K_α at 1.74 keV, and Ca-K_α at 3.69 keV).

According to the elemental analysis obtained by EDX, the films are close to the stoichiometric formula of PbS, where the Pb:S ratio is 1:1. The composition of PbS films is shown in Table 2. Figure 3 shows the EDX spectrum of a thin PbS film grown for 2 min.

3.4. Optical Properties. Figure 4 shows the optical transmittance (T) and specular reflectance (R) for PbS thin films. The optical absorption coefficient (α) as a function of the photon energy ($h\upsilon$) was estimated from the transmittance and reflectance spectra data and film thickness (d) by considering

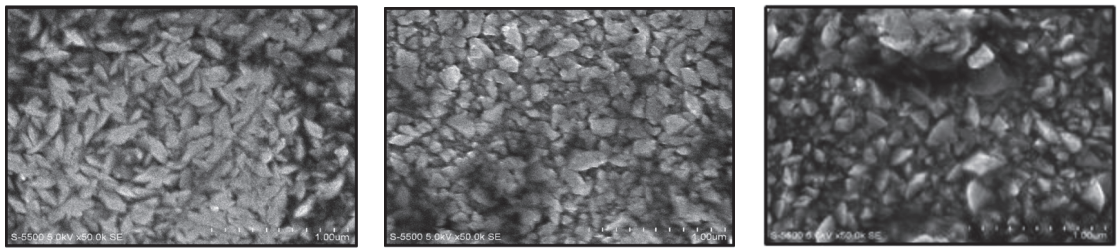

(a) (b) (c)

Figure 2: SEM images of PbS thin film grown for (a) 2 min, (b) 3 min, and (c) 4 min.

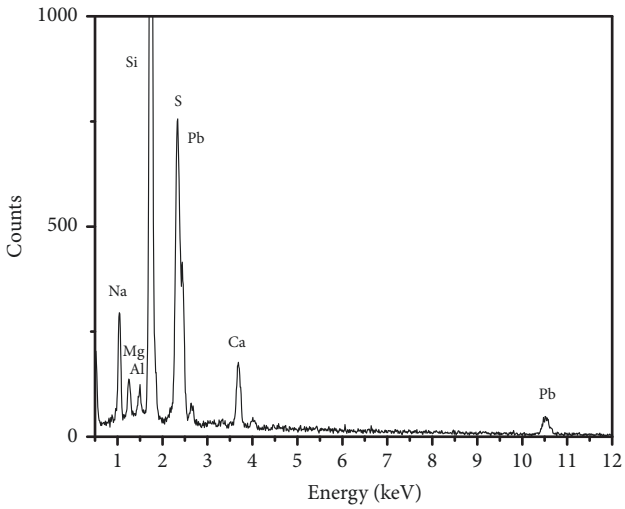

Figure 3: EDX spectrum of the PbS thin film grown for 2 min.

multiple reflections within the thin film, according to the following equation [30]:

$$\alpha = \frac{1}{d} \ln \left\{ \frac{(1-R)^2}{2T} + \left[\left(\frac{(1-R)^2}{2T} \right)^2 + R^2 \right]^{1/2} \right\}. \quad (6)$$

Figure 5 shows the optical absorption coefficient (α) of the PbS thin films. Plots of $(\alpha h\nu)^{2/3}$ versus hυ were used to calculate the energy values of the band gap by the linear fitting of the experimental data, as shown in the inset of Figure 4. The straight line region in this plot indicates that the absorption edge corresponds to a direct forbidden electronic transition as reported for PbS thin films grown by chemical bath deposition [31]. To understand the type of electronic transition which occurs during the optical absorption, $(\alpha h\nu)^2$ versus hν was also plotted. The best fit is obtained for $(\alpha h\nu)^{2/3}$ versus hν with a correlation factor of 0.99, while for plots of $(\alpha h\nu)^2$ versus hν the correlation factor decreases to 0.92 or less. Hence our experimental results suggest that optical band gap in PbS thin films has a direct band gap and forbidden electronic transitions taking place during the optical absorption [32].

The value of E_g was obtained when the adjusting line tends to zero ($\alpha \longrightarrow 0$). Values of $\alpha > 10^4$ cm^{-1} were obtained

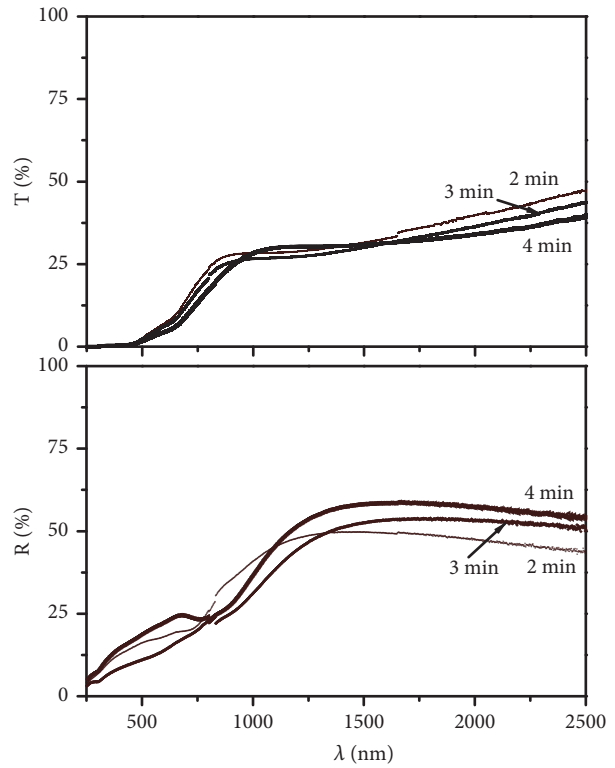

Figure 4: Transmittance (T) and reflectance (R) spectra for the PbS thin films at different thicknesses.

for the thin films, as displayed in Figure 4. The optical band gap values of the PbS thin films calculated were 1.35, 1.16, and 1.0 eV for 2, 3, and 4 min, respectively. The E_g value decreases with an increase in time deposition and this is likely to be attributed to an increase in crystal size, as is displayed in Table 1. Band gap values are in agreement with the values reported in the literature [5, 14].

3.5. Electrical Properties. Photoconductivity response curves of the films are shown in Figure 6. All the samples are slightly photoconductive. Electrical conductivity (σ) was estimated from the current and voltage values, the electrode geometry, and the film thickness. PbS thin films show a decrease in dark conductivity with an increase in time deposition. In polycrystalline semiconductors, the conductivity depends on

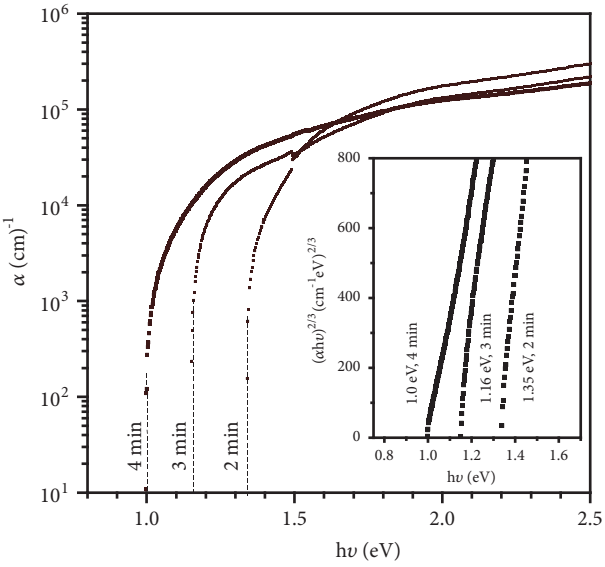

Figure 5: Optical absorption coefficient (α) of PbS thin films. Inset shows optical band gap values.

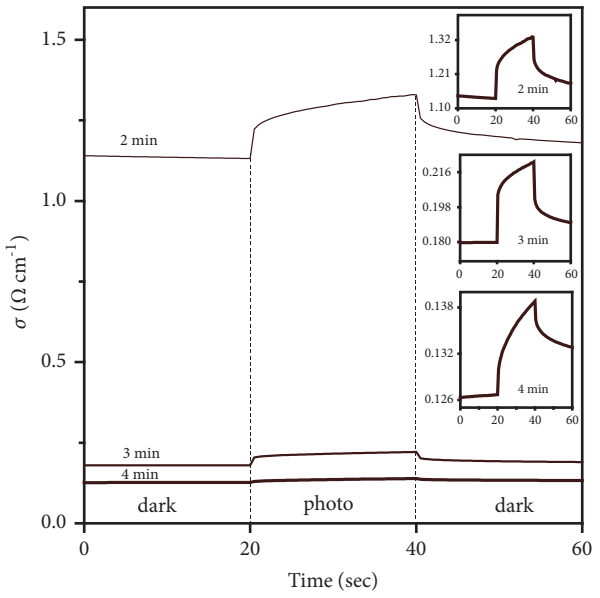

Figure 6: Electrical conductivity of PbS thin films. Inset shows the photoconductivity rise and decay.

three factors: (*i*) density of carriers, (*ii*) mobility, and (*iii*) potential barrier at the grain boundaries [33, 34]. Despite the absence of Kelvin probe force microscopy (KPFM) measurements of the films in this current communication, a comparison with other semiconducting polycrystalline systems led us to elaborate on potential causes behind the drop in conductivity [35–38]. The carrier conductivity of the samples might be analyzed assuming the "polycrystalline model," where carriers pass over back-to-back Schottky barriers that are generated by traps at grain boundaries (GB) via thermionic emission. These traps (charged defect states at GB) might result from impurities segregated during the thin film growth process. Moreover, for small grains, the mean free path of carriers is expected to be smaller than the width of barriers, and effects of carrier diffusion should play out also. Table 3 displays the values of electrical conductivity.

The Seebeck coefficients, S (μV K^{-1}), calculated from the thermoelectric measurements, are presented in Table 3. For all samples S is positive, indicating p-type conductivity. The Seebeck coefficient and the electrical conductivity are linked through an inverse relation [39]; i.e., the lower σ, the higher its S.

Hole concentration (p) was calculated through the following relation [40]:

$$S = \frac{k_B}{e}\left[\frac{5}{2} - s + \ln\frac{N_v}{p}\right], \tag{7}$$

where S is the Seebeck coefficient, s is the parameter which describes the scattering processes in the semiconductors, N_v is related to the density of states in the valence band, k_B is the Boltzmann constant, and e is the electron charge. According to the literature we assume the values of s as 5/2 and N_v as 10^{24} m^{-3} [39, 41]. Additionally, hole mobility (μ_p) was calculated from the relation between the conductivity and the hole concentration. Table 3 presents these results. The obtained results of μ_p for PbS thin films are in agreement with the value of 0.03x10^{-2} m^2 V^{-1} s^{-1} reported previously [31].

The relationship between the electrical conductivity and temperature is governed by the following equation [30]:

$$\sigma(T) = \sigma_o \exp\left(-\frac{E_a}{k_B T}\right), \tag{8}$$

where σ_o is a parameter whose value depends on the semiconducting material, E_a is the thermal activation energy, and k_B is the Boltzmann constant. In Figure 7 the dependence of ln (I) as a function of the inverse of the temperature (T) is plotted for PbS thin films. The Arrhenius plot yields a straight line, with the slope corresponding to the value of activation energy. The activation energies for the interval between 330 and 360 K are 0.14, 0.33, and 0.35 eV for deposition times of 2, 3, and 4 min, respectively. It is worth noticing that in polycrystalline materials the activation energy provides a measure of the Fermi energy (E_F), the maximum of the energy for the valence band (E_V), and the energy of the potential barrier of the grain boundaries (E_B), through the relationship $E_a = E_F - E_V + E_B$ [33].

4. Conclusions

The thin films of PbS were grown by the microwave-assisted chemical bath deposition (MA-CBD) technique in a commercial automated system. We were able to reduce the deposition times to less than 5 minutes and obtain films with good adhesion and homogeneousness throughout the surface of the substrate with thickness from 100 to 150 nm. The XRD analysis confirmed the polycrystalline cubic rock salt (NaCl) type structure with crystallite size between 18 and 20 nm as the deposition time was varied from 2 to 4 min. The EDX analysis indicates that the thin films were stoichiometric. All

Table 3: Electrical parameters of PbS thin films.

Sample	σ ($10^2 \Omega^{-1}$ m^{-1})		S (μV K^{-1})	p (10^{23} m^{-3})	μ_p (10^{-2} m^2 V^{-1} s^{-1})
	Dark	Illumination			
2 min	1.13	1.30	15	8.5	0.13
3 min	0.18	0.23	18	8.1	0.03
4 min	0.13	0.14	19	8.0	0.02

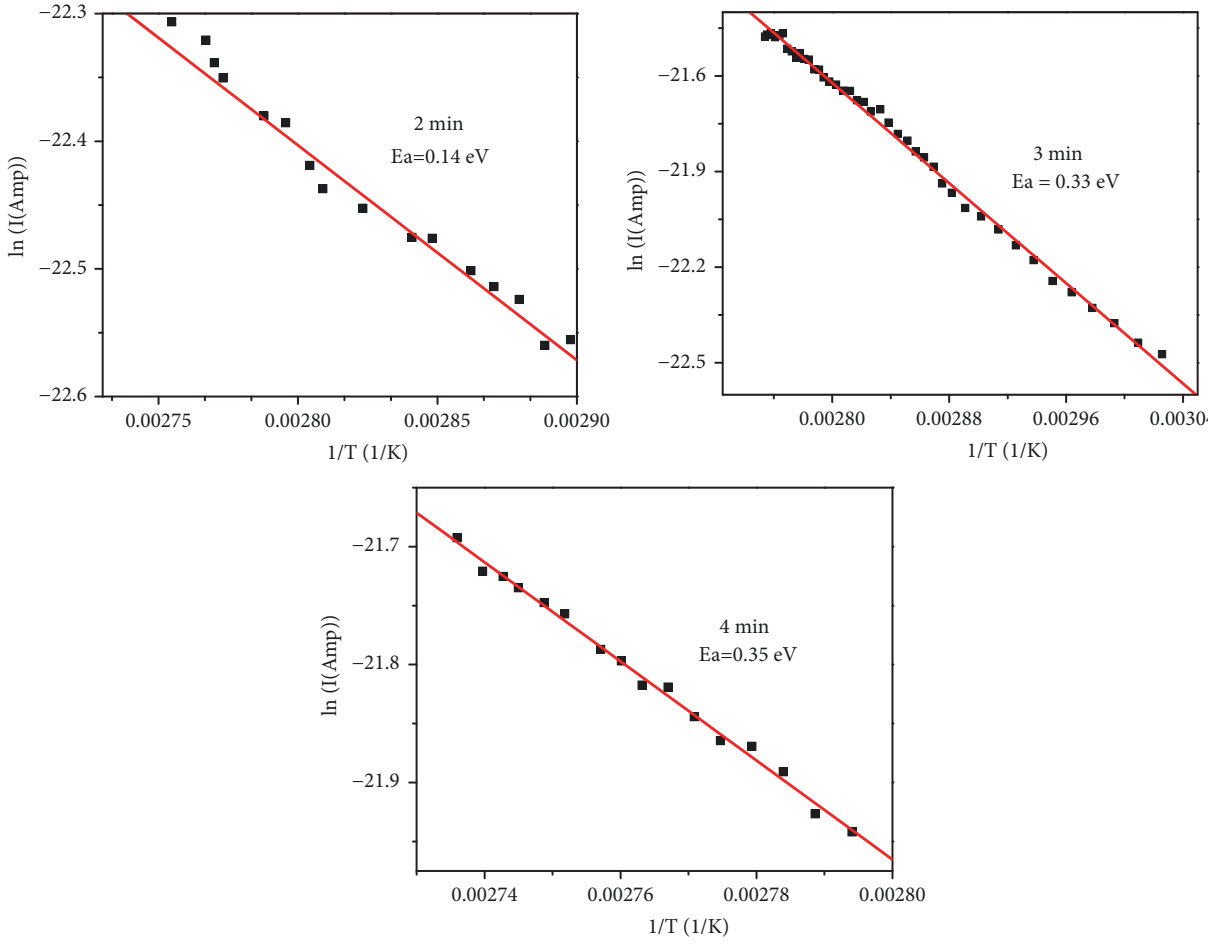

Figure 7: Plots of ln (I) *vs* ($1/T$) of PbS thin film as a function of deposition time.

the PbS films exhibit a direct band gap which varies from 1.0 to 1.35 eV. The films are of p-type conductivity with electrical conductivity in the range from 13 to 113 Ω^{-1} m^{-1}. Besides, hole mobility decreases from 0.13 x 10^{-2} to 0.02 x 10^{-2} m^2 V^{-1} s^{-1} with increasing deposition time. On the basis of the results, these thin films may be considered as potential candidates for optoelectronic applications.

Data Availability

The data used to support the findings of this study are available from the corresponding author upon request.

Conflicts of Interest

The authors declare that there are no conflicts of interest regarding the publication of this article.

Acknowledgments

We appreciate Yareli Colin Garcia's assistance in the optical measurements. We thank IER-UNAM through CONACYT-LIFYCS 123122 for infrastructure support. This work was supported by PRODEP (UAN-PTC-065 and UAN-PTC-062), CeMIE-Sol project 35, and Patronato UAN through the projects "Impulso a la Investigación."

References

[1] X. Liu and M. Zhang, "Studies on PbS and PbSe detectors for IR system," *Journal of Infrared, Millimeter, and Terahertz Waves*, vol. 21, p. 1697, 2000.

[2] S. Gunes, K. P. Fritz, H. Neugebauer, N. S. Sariciftci, S. Kumar, and G. D. Scholes, "Hybrid solar cells using PbS nanoparticles," *Solar Energy Materials and Solar Cells*, vol. 91, p. 420, 2007.

[3] J. Hernández-Borja, Y. V. Vorobiev, and R. Ramírez-Bon, "Thin film solar cells of CdS/PbS chemically deposited by an ammonia-free process," *Solar Energy Materials and Solar Cells*, vol. 9, p. 1882, 2011.

[4] S. M. Pawar, B. S. Pawar, J. H. Kim, O.-S. Joo, and C. D. Lokhande, "Recent status of chemical bath deposited metal chalcogenide and metal oxide thin films," *Current Applied Physics*, vol. 11, p. 117, 2011.

[5] T. Tohidi, K. Jamshidi-Ghaleh, A. Namdar, and R. Abdi-Ghaleh, "Comparative studies on the structural, morphological, optical, and electrical properties of nanocrystalline PbS thin films grown by chemical bath deposition using two different bath compositions," *Materials Science in Semiconductor Processing*, vol. 25, p. 197, 2014.

[6] B. Thangaraju and P. Kaliannan, "Spray pyrolytically deposited PbS thin films," *Semiconductor Science and Technology*, vol. 15, p. 849, 2000.

[7] A. Bednarkiewicz, D. Wawrzynczyk, M. Nyk, and W. Strek, "Optical, structural and optoelectronic properties of pulsed laser deposition PbS thin film," *Applied Physics B*, vol. 103, p. 161, 2011.

[8] S. Kumar, T. P. Sharma, M. Zulfequar, and M. Husain, "Characterization of vacuum evaporated PbS thin films," *Physica B: Condensed Matter*, vol. 325, pp. 8–16, 2003.

[9] J. P. Ge, J. Wang, H. X. Zhang, X. Wang, Q. Peng, and Y. D. Li, "Orthogonal PbS nanowire arrays and networks and their raman scattering behavior," *Chrmistry A European Journal*, vol. 11, p. 1889, 2005.

[10] P. T. Zhao, G. Chen, Y. Hu et al., "Preparation of dentritic PbS nanostructures by ultrasonic method," *Journal of Crystal Growth*, vol. 303, p. 632, 2007.

[11] K. K. Nanda and S. N. Sahu, "One-dimensional quantum confinement in electrodeposited PbS nanocrystalline semiconductors," *Advanced Materials*, vol. 13, p. 280, 2001.

[12] M. A. Barote, A. A. Yadav, T. V. Chavan, and E. U. Masumdar, "Characterization and photoelectrochemical properties of chemical bath deposited n-PbS thin films," *Digest Journal of Nanomaterial Biostructures*, vol. 6, p. 979, 2011.

[13] H. A. Pineda-Leon, G. Gutierrez-Heredia, A. De Leon et al., "Comparative study of PbS thin films growth by two different formulations using chemical bath deposition," *Chalcogenide Letters*, vol. 13, no. 4, pp. 161–168, 2016.

[14] C. E. Pérez-García, R. Ramírez-Bon, and Y. V. Vorobiev, "PbS thin films growth with CBD and PCBD techniques: a comparative study," *Chalcogenide Letters*, vol. 12, p. 579, 2015.

[15] A. S. Obaid, Z. Hassan, M. A. Mahdi, and M. Bououdina, "Characterization of nanocrystalline PbS thin films prepared using microwave-assisted chemical bath deposition," *Materials Science in Semiconductor Processing*, vol. 15, p. 564, 2012.

[16] T. Ding and J. Zhu, "Microwave heating synthesis of HgS and PbS nanocrystals in ethanol solvent," *Materials Science and Engineering: B Advanced Functional Solid-State Materials*, vol. 100, no. 3, pp. 307–313, 2003.

[17] Y. Zhao, X. H. Liao, J. M. Hong, and J. J. Zhu, "Synthesis of lead sulfide nanocrystals via microwave and sonochemical methods," *Materials Chemistry and Physics*, vol. 87, p. 149, 2004.

[18] M. Yousefi, M. Sabet, M. Salavati-Niasari, and H. Emadi, "Synthesis and characterization PbS and Bi_2S_3 nanostructures via microwave approach and investigation of their behaviors in solar cell," *Journal of Cluster Science*, vol. 23, p. 511, 2012.

[19] A. S. Obaid, Z. Hassan, M. A. Mahdi, and M. Bououdina, "Fabrication and characterisations of n-CdS/p-PbS heterojunction solar cells using microwave-assisted chemical bath deposition," *Solar Energy*, vol. 89, p. 143, 2013.

[20] H. Wang, J.-R. Zhang, and J.-J. Zhu, "A microwave assisted heating method for the rapid synthesis of sphalrite-type mercury sulfide nanocrystals with different sizes," *Journal of Crystal Growth*, vol. 233, p. 829, 2001.

[21] M. Xin, K. Li, and H. Wang, "Synthesis of CuS thin films by microwave assisted chemical bath deposition," *Applied Surface Science*, vol. 256, p. 1436, 2009.

[22] W. Tu and H. Liu, "Rapid synthesis of nanoscale colloidal metal clusters by microwave irradiation," *Journal of Materials Chemistry*, vol. 10, no. 9, pp. 2207–2211, 2000.

[23] S. Messina, M. T. S. Nair, and P. K. Nair, "Solar cells with Sb_2S_3 absorber films," *Thin Solid Films*, vol. 517, no. 7, pp. 2503–2507, 2009.

[24] B. Altıokka, M. C. Baykul, and M. R. Altıokka, "Some physical effects of reaction rate on PbS thin films obtained by chemical bath deposition," *Journal of Crystal Growth*, vol. 384, p. 50, 2013.

[25] E. Pentia, L. Pintilie, T. Botila, I. Pintilie, A. Chaparro, and C. Maffiotte, "Bi influence on growth and physical properties of chemical deposited PbS films," *Thin Solid Films*, vol. 434, no. 1-2, pp. 162–170, 2003.

[26] M. A. Mahdi, Z. Hassan, S. S. Ng, J. J. Hassan, and S. K. M. Bakhori, "Structural and optical properties of nanocrystalline CdS thin films prepared using microwave-assisted chemical bath deposition," *Thin Solid Films*, vol. 520, no. 9, pp. 3477–3484, 2012.

[27] R. M. Palou, "Microwave-assisted synthesis using ionic liquids," *Molecular Diversity*, vol. 14, no. 1, pp. 3–25, 2010.

[28] E. Yücel, N. Güler, and Y. Yücel, "Optimization of deposition conditions of CdS thin films using response surface methodology," *Journal of Alloys and Compounds*, vol. 589, p. 207, 2014.

[29] M. M. Abbas, A. A.-M. Shehabb, N.-A. Hassanb, and A.-K. Al-Samuraee, "Effect of temperature and deposition time on the optical properties of chemically deposited nanostructure PbS thin films," *Thin Solid Films*, vol. 519, p. 4917, 2011.

[30] D. K. Schroder, *Semiconductor Materials and Device Characterization*, Wiley, New York, NY, USA, 2nd edition, 1990.

[31] H. Moreno-García, M. T. S. Nair, and P. K. Nair, "Chemically deposited lead sulfide and bismuth sulfide thin films and Bi2S3/PbS solar cells," *Thin Solid Films*, vol. 519, no. 7, pp. 2287–2295, 2011.

[32] J. I. Pankove, *Optical Processes in Semiconductors*, Dover, New York, NY, USA, 2nd edition, 1975.

[33] J. W. Orton, B. J. Goldsmith, J. A. Chapman, and M. J. Powell, "The mechanism of photoconductivity in polycrystalline cadmium sulphide layers," *Journal of Applied Physics*, vol. 53, no. 3, pp. 1602–1614, 1982.

[34] J. Y. W. Seto, "The electrical properties of polycrystalline silicon films," *Journal of Applied Physics*, vol. 46, no. 12, pp. 5247–5254, 1975.

[35] E. Canessa and V. L. Nguyen, "Non-linear I–V characteristics of double Schottky barriers and polycrystalline semiconductors," *Physica B: Condensed Matter*, vol. 179, no. 4, pp. 335–341, 1992.

[36] R. Matsubara, N. Ohashi, M. Sakai, K. Kudo, and M. Nakamura, "Analysis of barrier height at crystalline domain boundary and in-domain mobility in pentacene polycrystalline films on SiO2," *Applied Physics Letters*, vol. 92, no. 24, p. 242108, 2008.

[37] R. Baier, C. Leendertz, D. Abou-Ras, M. C. Lux-Steiner, and S. Sadewasser, "Properties of electronic potential barriers at grain boundaries in Cu(In,Ga)Se_2 thin films," *Solar Energy Materials and Solar Cells*, vol. 130, pp. 124–131, 2014.

[38] T. Kamiya, Z. A. K. Durrani, and H. Ahmed, "Reduction of grain-boundary potential barrier height in polycrystalline silicon with hot H_2O-vapor annealing probed using point-contact devices," *Journal of Vacuum Science & Technology B*, vol. 21, p. 1000, 2003.

[39] S. M. Sze, *Physics of Semiconductors Devices*, Wiley, New York, NY, USA, 2nd edition, 1981.

[40] R. A. Smith, *Semiconductors*, Cambridge University Press, Cambridge, UK, 2nd edition, 1978.

[41] K. Bindu, J. Campos, M. T. S. Nair, A. Sanchez, and P. K. Nair, "Semiconducting $AgSbSe_2$ thin film and its application in a photovoltaic structure," *Semiconductor Science and Technology*, vol. 20, p. 496, 2005.